Freestanding and scalable force-softness bimodal sensor arrays for haptically body feature identification

Zequn Cui, Wensong Wang, Huarong Xia, Changxian Wang, Jiaqi Tu, Shaobo Ji, Joel Ming Rui Tan, Zhihua Liu, Feilong Zhang, Wenlong Li, Zhisheng Lv, Zheng Li, Wei Guo, Nien Yue Koh, Kian Bee Ng, Xue Feng, Yuanjin Zheng, Xiaodong Chen**

Z. Cui, H. Xia, C. Wang, J. Tu, S. Ji, F. Zhang, Z. Li, W. Guo, X. Chen
Innovative Centre for Flexible Devices (iFLEX) & Max Planck–NTU Joint Lab for Artificial Senses, School of Materials Science and Engineering, Nanyang Technological University, 50 Nanyang Avenue, Singapore 639798, Singapore
E-mail: chenxd@ntu.edu.sg

W. Wang, Y. Zheng
School of Electrical & Electronic Engineering, Nanyang Technological University, 50 Nanyang Avenue, Singapore 639798, Singapore
E-mail: yjzheng@ntu.edu.sg

J. Tu
Institute of Flexible Electronics Technology of THU, Zhejiang, Jiaxing, 314000 China

J. M. R. Tan
School of Materials Science and Engineering, Nanyang Technological University, 50 Nanyang Avenue, Singapore 639798, Singapore

Z. Liu, W. Li, Z. Lv, X. Chen
Institute of Materials Research and Engineering, the Agency for Science, Technology and Research, 2 Fusionopolis Way, Innovis, #08-03, Singapore 138634, Singapore

N. Y. Koh, K. B. Ng
Lee Kong Chian School of Medicine, Novena Campus, Nanyang Technological University, 11 Mandalay Road, Singapore 308232, Singapore

X. Feng
Laboratory of Flexible Electronics Technology, Tsinghua University, Beijing, 100190, China

X. Chen
Institute for Digital Molecular Analytics and Science (IDMxS), Nanyang Technological University, 59 Nanyang Drive, Singapore 636921, Singapore

Keywords: Body feature identification, tactile gloves, pressure sensors, softness sensing, palpation

Tactile technologies that can identify human body features are valuable in clinical diagnosis and human-machine interactions. Previously cutting-edge tactile platforms can identify structured non-living objects; however, human body feature identification remains challenging mainly because of the irregular contour and heterogeneous spatial distribution of softness. Here we develop freestanding and scalable tactile platforms of force-softness bimodal sensor arrays, enabling tactile gloves to identify body features using machine learning methods. The bimodal sensors are engineered by adding a protrusion on a piezoresistive pressure sensor, endowing the resistance signals with combined information of pressure and the softness of samples. The simple design enables 112 bimodal sensors to be integrated into the thin, conformal, and stretchable tactile glove, allowing the tactile information to be digitalized while hand skills are performed on the human body. The tactile glove shows high accuracy (98%) in identifying four body features of a real person, and four organ models (healthy and pathological) inside an abdominal simulator, demonstrating body feature identification of the bimodal tactile platforms and showing their potential use in future healthcare and robotics.

1. Introduction

The identification of the human body features by touch is critical for the clinic and human-robot interactions.[1-20] For example, doctors commonly palpate a patient's body by feeling the softness using their hands and fingers to assess the exact pain locations for diagnostic evaluation and to locate specific anatomic structures and abnormalities during surgery.[21] New-generation social robots are required to interact with people smoothly and naturally and to obtain social-cognitive skills including emotion-based body interactions,[22-24] e.g. recognizing and interpreting the personality and affective information of a person during a handshake because the hand features and gripping forces vary from individuals and psychological status.[25, 26] Digitalizing the touch-based identification process on the human body provides quantitative and objective results, which would revolutionize subjective and experience-based conventional palpation in the clinic, as well as facilitate the development of human-like social robots. To achieve this, a desirable approach is to develop tactile gloves fully covered with sensor arrays that can record tactile information during hand-body interactions.

Recently remarkable progress has shown that wearable sensor arrays with hundreds of pressure sensors can identify objects with various shapes and human-environment interactions using machine learning methods based on large-area tactile information.[27,28] Development of quadruple sensors allows sensing of four different types of mechanical and thermal information, and a robot hand integrated with only ten quadruple sensors enables garbage sorting with high

identification accuracy,[29] showing that increasing the sensing modalities of single sensors can significantly enhance the accuracy. Considering the irregular shape and heterogeneous spatial distribution of the softness in the human body, tactile sensor arrays that can sense large-area force and softness are desired for the identification of the human body. Although pressure sensor arrays have been widely developed and have shown the ability to differentiate the softness, they can only be considered as single softness devices.[10] The fabrication of tactile softness device arrays has been hindered because specialized tactile softness devices typically require deliberate design and complicated fabrication.[7, 21, 30-32] For example, a single stretchable strain sensor enables Young's modulus of soft materials to be measured simply by touching and independent of the touching forces, which requires the fabrication of millimeter-scale three-dimensional self-locked structures.[7] Therefore, scalable fabrication of high-density force and softness bimodal sensor arrays remains challenging.

Here, we develop freestanding and scalable wearable tactile platforms of force-softness bimodal sensor (FSS) arrays. The bimodal tactile platforms can be tailored according to target subjects, yielding a tactile glove fully covered with 112 FSSs that can identify body features using machine learning methods. The FSS is designed for sensing the combined information of pressure and the softness of samples, which is achieved by simply adding a protrusion on top of a piezoresistive pressure sensor. Based on data analysis from multiple tests, a single FSS can differentiate the softness of different samples. The design contributes to a thin (< 1 mm), conformal and stretchable tactile glove that features large-area force and softness sensing and allows for finger dexterity and the natural sense of touch. A comparison between our tactile glove with other tactile gloves has been presented in Table S1. Combined with a support vector machine classifier, which is a supervised machine learning algorithm, our tactile glove identifies four body parts in a real person and four healthy and pathological organ models in a medical abdominal simulator with high accuracy (98%). This work demonstrates a bimodal tactile platform for digitalizing the interaction with the human body and identifying body features, showing the potential use for establishing objective diagnostic approaches in the clinic and advanced tactile systems for robotics.

2. Results and discussion

2.1. Freestanding and scalable force-softness bimodal tactile platforms

In principle, a pressure sensor made of a piezoresistive film on a pair of interdigital electrodes can only detect pressure (**Figure 1**a, i). When different samples with varied softness

are pressed on the sensor, the resistance signal is only dependent on the pressing force (F_{tot}) and independent of the materials (Figure 1b, i). However, when a protrusion is added to the pressure sensor (Figure 1a, ii), the resistance experiences two phases (p_1 and p_2) and is dependent on both the total pressing force (F_{tot}) and Young's modulus (E) of the samples (Figure 1b, ii). The mechanism is presented in Figure 1c. In p_1, both softer and harder samples are pressed on the protrusion with the same total pressing forces (F_{tot}) without touching the substrate, yielding the same forces applied on the protrusion (F_p, $F_{p\text{-}s} = F_{p\text{-}h} = F_{tot}$), and no force exerted on the substrate (F_s, $F_{s\text{-}s} = F_{s\text{-}h} = 0$). With the increasing pressing forces (moment t_0), the softer sample deforms more and comes into contact with the substrate (with a touching force $F_{s\text{-}s} = 0$) as compared to the harder sample ($F_{p\text{-}s} = F_{p\text{-}h}$). With further increase of the pressing forces (moment t_1), more pressing force on the softer sample is shared by the substrate ($F_{s\text{-}s} > 0$), while the harder sample comes into contact with the substrate ($F_{s\text{-}h} = 0$), leading to an actual smaller force on the protrusion for the softer sample ($F_{p\text{-}s} < F_{p\text{-}h}$) and consequently a higher resistance signal ($R_s > R_h$). The trend follows when the pressing forces (moment t_2) are increased further, leading to higher resistance for the softer sample ($F_{p\text{-}s} < F_{p\text{-}h}$, $R_s > R_h$). Therefore, the sample softness can be deduced from the resistance change of the pressure sensor with a protrusion; the softer the sample, the higher the resistance under the same pressing forces. Detailed theoretical analysis was presented and a universal equation between the force exerted on the protrusion (F_p), the total force (F_{tot}), and Young's modulus of the samples (E) was established (Note S1 and Figure S1, S2, Supporting Information).

Based on the simple principle, a freestanding, scalable, conformal, and stretchable tactile platform with 200 FSSs distributed in a large area (120 mm × 235 mm) can be fabricated using industrial adaptable processes (Figure 1d and Figure S3). To enable correct force and softness mapping, a co-grounded individual channel routing method (COIN) was used for the electrode design (Figure S4). This means all 200 sensors share only 1 common electrode and each an individual counter electrode, yielding a total of 201 electrodes. The COIN allows each sensor to be tuned, collected, and calibrated individually, avoiding the crosstalk effect and enabling correct tactile mapping.[27, 28] Moreover, the design increases system reliability against possible cascading effects from single points damage. Figure 1e schematically presents the architectural design of a single sensing unit. Coaxial circular electrodes were designed in each unit, and the outer electrode was electrically connected with the counter electrode while the inner one was connected with the common electrode through via holes. Commercial piezoresistive films (Velostat, 3M) were punctured into circular sheets and were adherent to the coaxial circular

electrodes by hot-press. The films were then sealed to avoid peeling off, and a hemispherical protrusion adhered to the top.

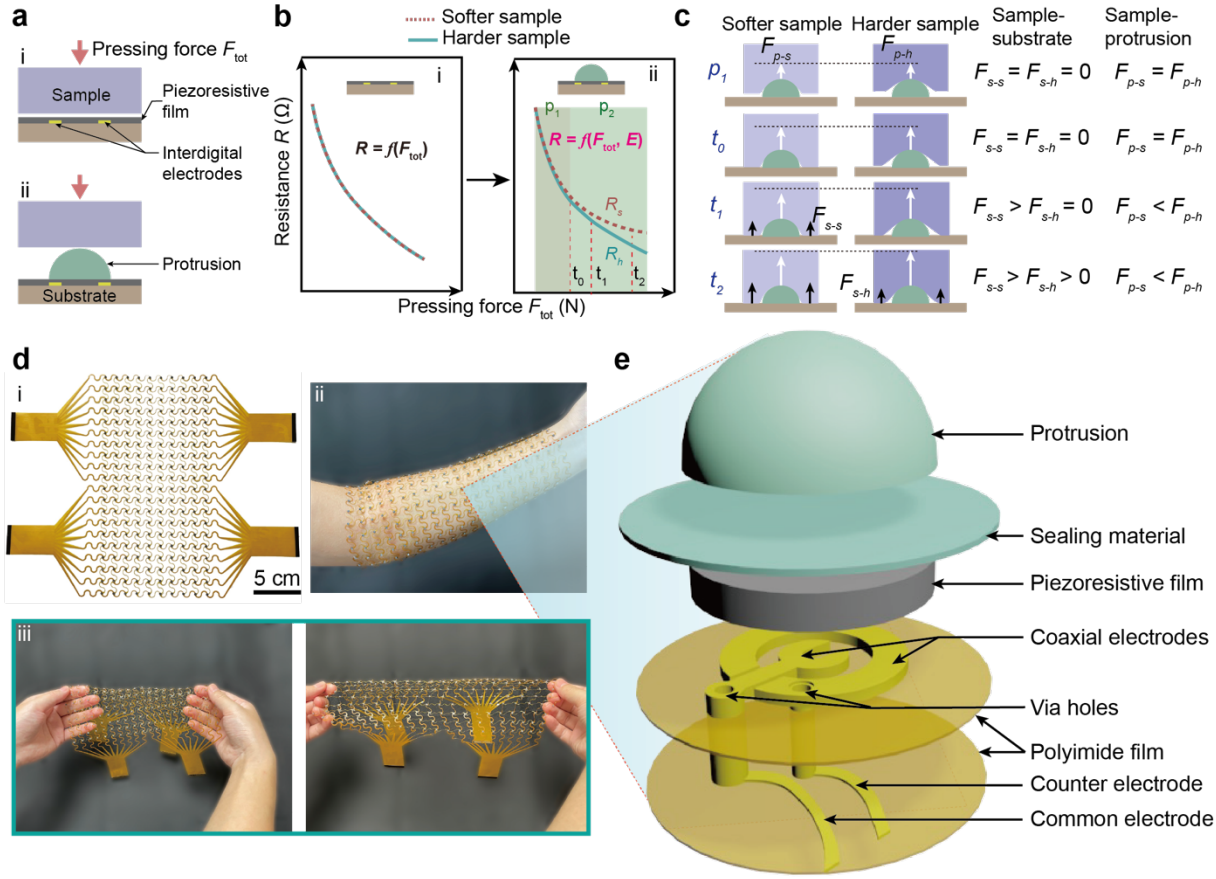

Figure 1. The force-softness bimodal sensing mechanism of the FSS and the freestanding and scalable bimodal tactile platform. a) Schematic showing pressure sensors without (i) and with (ii, FSS) a hemispherical protrusion on the top pressed by a sample. The pressure sensor is made of a piezoresistive film placed on a pair of interdigital electrodes. b) Graphs indicate the difference in resistance change between the two sensors when samples with different softness (Young's moduli) are pressed on them. The FSS can identify the different samples (ii), while the pressure sensor cannot (i). c) Schematic showing the mechanism of softness identification of the FSS. Softer samples lead to higher resistances of the sensor than harder ones under the same pressing forces. p_1, the phase that both softer and harder samples only touch protrusion but not substrate. t_0, the time when the softer sample starts to touch the substrate, but the harder sample does not. t_1, the time when the harder sample starts to touch the substrate. t_2, the time after both samples touch the substrate. F_{s-s}, force on substrate pressed by softer sample. F_{s-h}, force on substrate pressed by harder sample. F_{p-s}, force on protrusion pressed by softer sample. F_{p-h}, force on protrusion pressed by harder sample. d) Photos showing a freestanding, scalable (i), conformal (ii), and stretchable (iii) sensor array with 200 FSSs. e) Schematic showing the architectural design of a single sensing unit. The piezoresistive film adheres to a pair of coaxial circular electrodes, which connect with the common electrode and the counter electrode through via holes, respectively. The piezoresistive film is further sealed, and a hemispherical protrusion adheres on the top.

2.2. Properties of the FSSs

To demonstrate the bimodal sensing of our FSSs, circular interdigital electrodes (chromium (Cr, 3 nm)/gold (Au, 100 nm)) were fabricated on polyester (PET) films, and the

commercial piezoresistive film was adhered on the top using polyimide tapes (Figure S5a). This structure yields a pressure sensor with a non-linear mechanical-electrical relationship (Figure S6), and adding a protrusion to it forms the FSS. The FSS was pressed by six different samples with the same pressing speed before the pressing force reaches 20 N, which was under the control of a commercial mechanical testing system (Figure S5b, c).

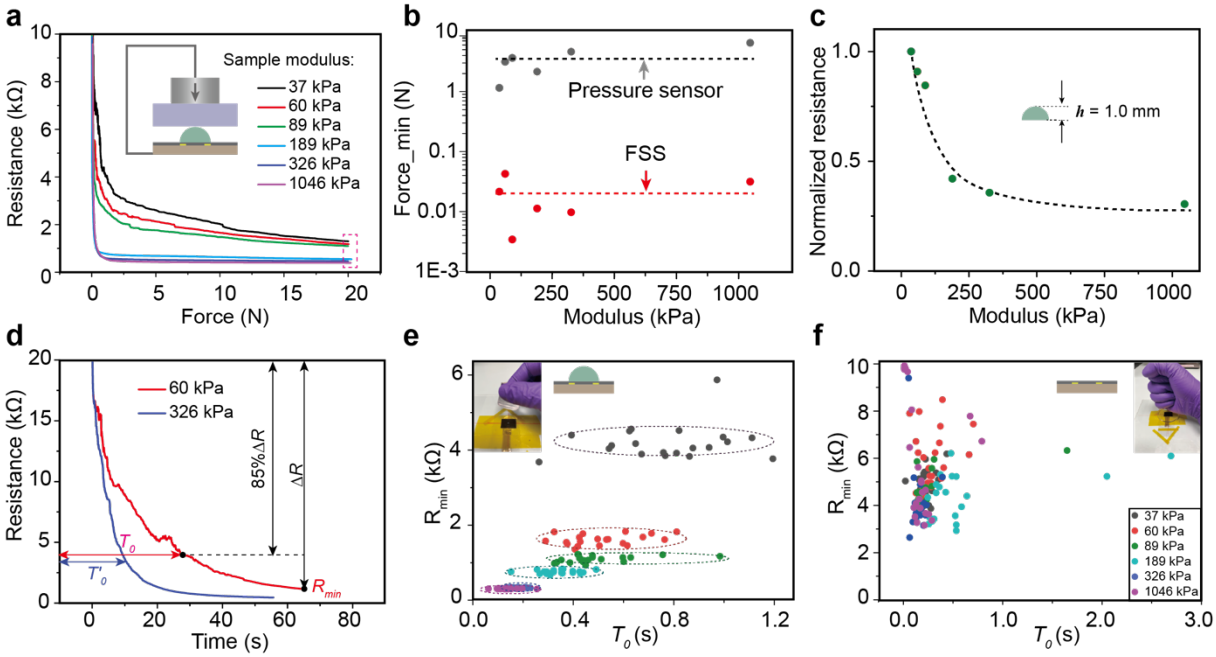

Figure 2. Properties of the FSS. a) Resistance of the FSS decreases differently under the pressing of six different samples controlled by a mechanical testing machine (schematically shown in the inset). Different colored curves indicate samples with different Young's moduli. b) The minimum response forces of the FSSs are ~2 orders of magnitude lower than those of the pressure sensors. c) Normalized resistances of the FSS when pressed by different samples at 20 N (red dashed box in (a)) showing that the resistance decreases with the increase of samples' Young's moduli. d) The resistance-time curves of the FSS pressed by two different samples. Data are taken and transferred from (a). Two feature variables are extracted from each curve: R_{min}, the minimum resistance; T_0, the time that the resistance drops at 85% of the resistance change. Lower R_{min} indicates higher pressing forces for the same sample, while larger T_0 indicates softer samples. e, f) Comparison of the two feature variables between an FSS (e) and a pressure sensor (f) when pressed by six samples without the intentional control of a person, showing that the FSS identifies different softness, while the pressure sensor cannot. Different colored dots indicate different samples as indicated in (f).

Figure 2a highlights the differential resistance changes of the FSS when pressed by different samples: for the pressing of softer samples, the resistance drops slower at the initial stage and always remains higher than that of harder samples, indicating that the resistance signal involves the information of the pressing force and the softness of the samples, which proves our idea. The heights of the protrusions were investigated and were shown to have negligible influence on the trend of resistance change while they all contribute to enhanced sensitivity (Figure S7). The softness and the morphologies of the protrusion were also investigated and

showed no obvious influence on the FSS performance (Figures S8, S9). However, the flatness of the sample surface influenced the tests, and curved surfaces tended to cause smaller resistances (Figure S10). Thus the FSS with the hemispherical protrusion of 1 mm height and flat samples were selected for further study, which shows minimum detection forces that are much smaller than those of the pressure sensor (Figure 2b). Based on the minimum detection force (~20 mN), a minimum Young's moduli of samples was numerically calculated as 12 kPa (Figure S11). The resistances of the FSS at 20 N pressing forces decrease with the samples' Young's moduli (Figure 2c), demonstrating the sensing of the softness by the FSS. Since each resistance-force curve is correlated with the softness of the sample and the pressing force, both the softness and the pressing force can be deduced from the curve, suggesting bimodal sensing. However, in practical situations, a testing machine is not available, and the pressing condition (force and movement) would not be well controlled. Thus, what we can obtain is the resistance-time instead of the resistance-force relationship.

To adapt to the practical situations, we translate two resistance-force curves from Figure 2a into the resistance-time curves according to the pressing conditions of the testing machines (Figure 2d). The softer sample leads to higher resistance compared with the harder sample, and the resistance drops slower at the initial stage, of which the trends agree with the resistance-force curves. We then extracted the corresponding feature variables from the resistance-time curve to differentiate the softness of the samples: R_{min} and T_0. R_{min} is the minimum resistance under pressing, and T_0 is the time that the resistance drops at 85% of the resistance change. Therefore, for the same testing condition, T_0 is larger for softer materials, and R_{min} indicates the pressing force for the same sample. To show that the FSS can differentiate the softness of samples even without the control of a machine, both the FSS and the corresponding pressure sensor were pressed by the six samples without the intentional control of a person (Figure S5d). Although the pressing conditions would not be well controlled when a person manually operates the tests, multiple tests with unintentional control would yield similar testing conditions due to habitual actions. Each sample was pressed on either sensor around 20 times (Figure S12), and the features R_{min} and T_0 were extracted (Figure 2e, f). For the FSS, the feature values clustered together according to the pressed samples, indicating softness identification of the FSS without intentional human control (Figure 2e). Specifically, softer samples were easier to be identified. Compared with the FSS, the pressure sensor cannot differentiate the softness of the six samples (Figure 2f).

2.3. Performance of the scalable tactile glove

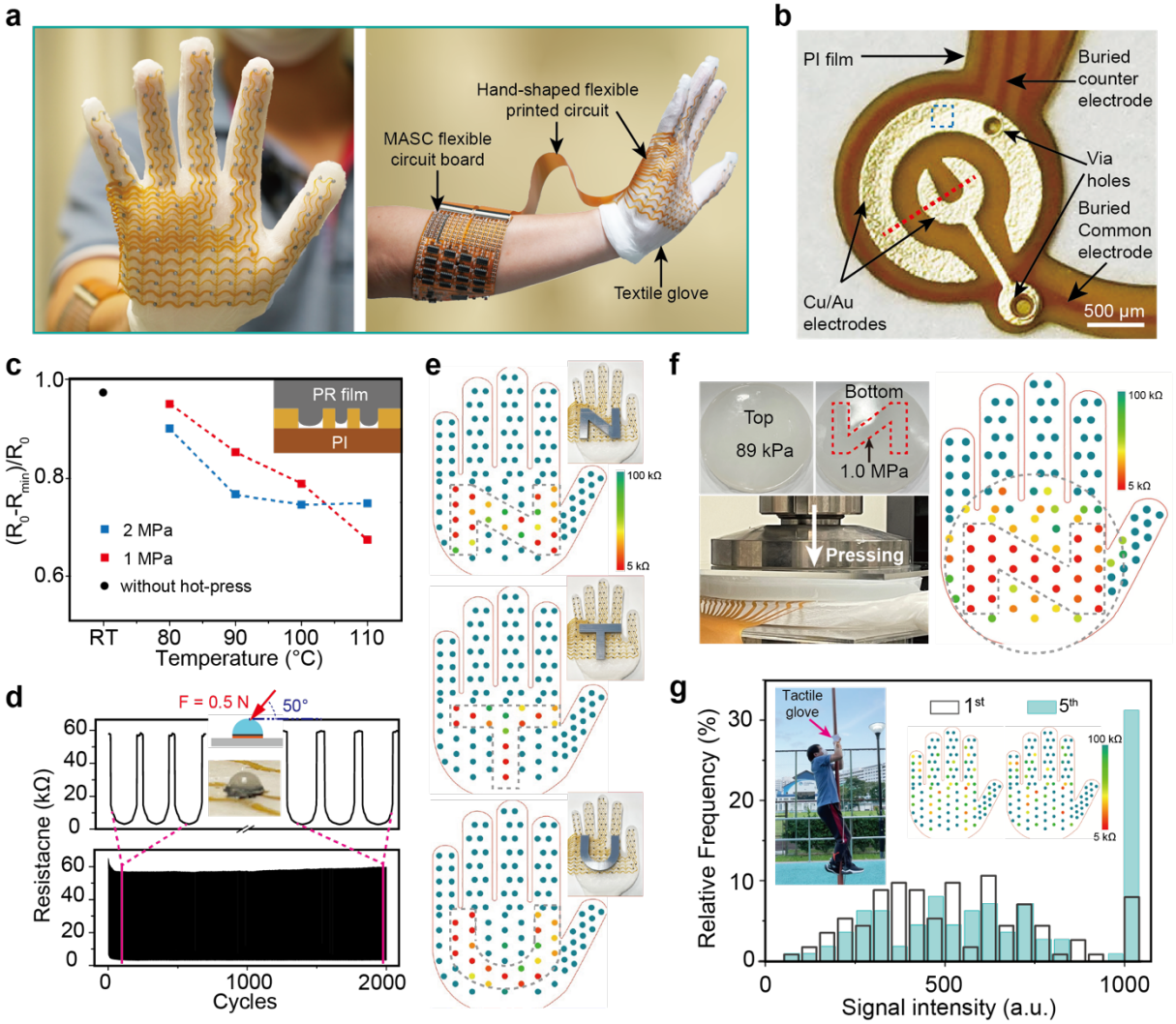

Figure 3. Structure and performance of the tactile glove. a) Photos showing the scalable tactile glove consisting of 112 FSSs and a MASC flexible circuit board is worn on the forearm. b) Photo showing the exposed coaxial circular electrodes, via holes, buried common electrode, and the counter electrode of the FSS for the tactile glove. c) Resistance changes of the piezoresistive pressure sensor fabricated from different hot-press conditions (pressure and temperature) under the pressing force of 2 N as indicated in Figure S8. Inset showing the interlocked structure between the piezoresistive (PR) film and the electrodes. d) Dynamic mechanical-electrical response of the FSS under tilted force (0.5 N @ 50°) with 2000 cycles show strong mechanical robustness. e) Tactile images show crosstalk-free tactile gloves when pressed by three models. f) A non-homogeneous sample (a harder mirrored "N" letter embedded in the bottom of a softer disk sample) was pressed on the tactile glove, showing softness mapping of the tactile glove. g) The tactile glove can withstand a person (~60 kg) climbing a pole for more than 5 times gripping action. Tactile images (insets) and signal intensities of all sensors of the tactile glove at 1st (blank bars) and 5th (light green bars) gripping were shown. Signal intensities larger than 1000 indicate non-touched or damaged sensors. The increased relative frequency from 1st (8%) to 5th (31%) gripping suggests that 77% of all sensors still worked well after 5 times gripping, showing the mechanical robustness of the tactile glove. The color bars in (e, f, g) indicate resistances ranging from 5 kΩ (red) to 100 kΩ (dark green).

To enable gloves with spatially tactile sensing of force and softness, the bimodal tactile platform was tailored into a hand shape and integrated into a textile glove, yielding a tactile glove. To remain finger dexterity and the natural sense of touch in hand activities, a textile

glove made of polyamide (PA) and polyurethane (PU) fibers was chosen as the substrate, yielding a thin (~0.88 mm) and conformal tactile glove (Figure S13). **Figure 3**a displays the scalable and conformal tactile glove with 112 FSSs and a light-weighted massive analog signal channel-based flexible printed circuit board (MASC-FPCB) worn on the arm for data collection. Figure 3b shows a pair of exposed coaxial circular electrodes and buried common and counter electrodes for each sensor. The electrodes have a surface roughness of ~1 μm (Figure S14b, c) and a thickness of ~18 μm (Figure S14d). The 18-μm-thick electrodes combined with coaxial circular design yielded mechanical robustness of the sensors: the interlocked structure was generated between the electrodes and the piezoresistive sheets as hot-press was applied (inset of Figure 3c and Figure S14e-f). The effects of hot-press on both mechanical-electrical performance and mechanical robustness were studied (Figure 3c, d, and Figure S15). As the softening temperature of the piezoresistive film is around 100 °C (Figure S14a), four temperatures ranging from 80 °C to 110 °C together with different pressure were applied in the hot-press. Results show that lower temperature and lower pressure in the hot-pressing lead to higher sensitivity (Figure 3c). Considering that higher temperature and higher pressure are more likely to generate the interlock structures and consequently enhance the robustness, trade-off parameters of 90 ℃ at 1 MPa were chosen in hot-press. The fabrication led to a good utility of pressure sensors with most initial resistances around 20 kΩ, which is much better than commonly used polydimethylsiloxane (PDMS) pyramid micro-structured pressure sensors,[33] as the coefficient of variation of the resistance of the former is almost one-third of the later (Figure S16). Sealing the pressure sensors using a mechanically robust commercial silicone gel (Figure S17) lowered the initial resistances of the pressure sensors slightly (Figure S16a, b), indicating normal forces generated to the pressure sensors by the sealing material, more than just protecting the surface. As a result, the FSSs are electrically and mechanically robust and can withstand both strong normal and shear forces. To show this, dynamic pressing was applied on the protrusion of an FSS with a tilted force (0.5 N @ 50°, test setup shown in Figure S18) for 2000 cycles (Figure 3d). The peak values decreased slightly in the previous dozens of cycles and maintained almost unchanged in the following cycles, showing reliable mechanical-electrical performance under both normal and shear forces, which is essential for practical use. As a comparison, the same tests were applied to the well-sealed PDMS pyramid micro-structured pressure sensors (Figure S19); however, the signals were unstable and changed largely after 500 cycles. The softness of the supporting platform was also investigated and showed that a softer platform yields higher resistance of the FSS sensor than a harder platform

under the same pressing forces (Figure S20). This indicates that the signals of the tactile glove would be weaker when worn on the hand while maintaining the softness distinction ability.

The glove is crosstalk-free as shown by pressing three models of "N", "T", and "U" on it (Figure 3e and Movie S1, Supporting Information). When a soft sample (E = 89 kPa) with harder materials (E = 1.0 MPa) patterned at the bottom was covered and pressed on the tactile glove with FSS arrays, softness mapping was obtained effortlessly (Figure 3f and Movie S2, Supporting Information), while the tactile image of a tactile glove with pressure sensor arrays didn't show a clear softness distribution at the same pressing condition (Figure S21).

Besides softness mapping, our tactile glove is robust enough to withstand frequently high-force pressing to meet the practical requirement. To show that the glove can withstand both large normal and shear forces, a person (~60 kg) wearing the glove climbed a pole with more than 5 times gripping action (Figure 3g and Movie S3, Supporting Information). Signals of all sensors at 1st and 5th gripping were statistically shown (Figure 3g). The increased relative frequency of signals larger than 1000 indicates that most sensors (77%) remained working after 5 times gripping. Together, the results demonstrate the mechanical robustness of the tactile glove that is adequate for practical usage.

2.4. Body feature identification

With the ability of softness identification and force sensing at each pixel, we expect the tactile glove to identify different body features of a real person (e.g. arm, shoulder, belly, chest (**Figure 4**a). Moreover, we intend to check the possibility of the tactile glove in identifying inner body features, which is commonly performed by doctors in the clinic to assess health and disease with palpation skills. To check the potential value for clinical usage, a medical abdominal simulator with four organ models (healthy and pathological liver and spleen) was prepared, and a palpation assessment on the simulator was conducted while wearing the tactile glove (Figures 4b and Movie S4, Supporting Information). The patterns of the tactile signals were not differentiable either in different human body features or in different organ models of the simulator, while they showed slight differences between the real body features and the simulator (Figures 4c); specifically, fewer sensors responded in the palm for the simulator. This is reasonable because we used the whole palm to press and hold the body parts of the real person, while we mostly used the fingers to press deeply and check the inner organs of the simulator.

To explore the body feature identification ability of our tactile glove, a machine learning method was leveraged. We applied 200 times pressing on each body part of the real person and 250 times pressing on each organ location of the simulator. We recorded 20–30 data during

each press for each sensor (Figure S22), yielding a total of 1800 files. Two features related to pressing force and pressing duration were extracted for each sensor in each press (Figure S23), leading to 224 selected feature values for each press, considered as one group of fine data. Therefore, after pre-processing and feature extraction, a total of 1800 groups of fine data were presented (Figure 4d). A support vector machine was trained with 80% of the above data and then was evaluated by the remained 20% of the data. The identification accuracy of single sensors was higher (most 30%–40%) than the baseline of random probability (12.5%), with a few sensors reaching ~60%, showing the superiority of our FSSs (Figure 4e). Relying on the unique features of the FSSs, the array with 112 sensors enabled the tactile glove with high accuracy of 98% to identify all the patterns (Figure 4f).

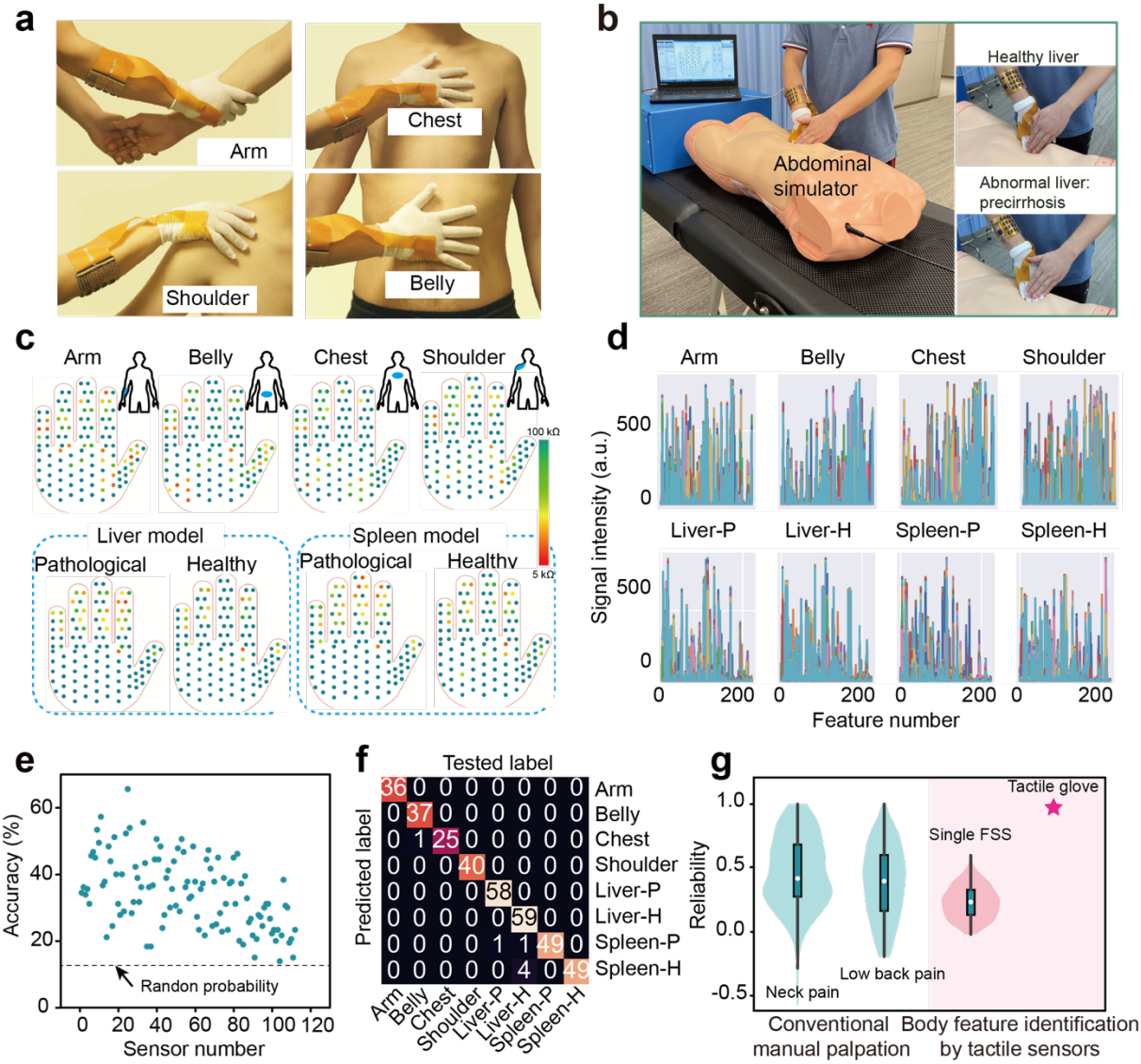

Figure 4. Body feature identification. a, b) Photos showing that the tactile glove was used to identify body parts of a real person (a) and organ models inside an abdominal simulator (b). c) Tactile signal patterns of four different body parts (arm, belly, chest, shoulder) of the real person (top) and four different organ models (healthy liver, pathological liver, healthy spleen, pathological spleen) of the abdominal simulator obtained by the tactile glove. The color bar

indicates resistance ranging from 5 kΩ (red) to 100 kΩ (dark green). d) Statistic of all 224 feature intensities during one pressing on each item cannot differentiate from each other. e) The accuracy of every single FSS of the tactile glove in identifying the eight items shows that most of them are much higher than the random probability of 12.5, with a few sensors reaching the accuracy of ~60%, showing the priority of the FSS. f) Machine learning results show high accuracy (98%) of the tactile glove in identifying the eight items. g) Comparison of the reliability (Kappa value) of body feature identification among conventional manual palpation, single FSSs, and the tactile glove. Manual palpation typically has lower reliability (~0.4) on real patients when identifying the pain locations of neck pain and low back pain.[35,36] The identification reliability of the single FSSs and the whole tactile glove on the four different body parts and the four artificial organ models achieves 0.2–0.3 and 0.98, respectively.

The above results show the effectiveness of the tactile glove in identifying human body features and the potential application for digitalized palpation assessment. This would be significant for the clinic because conventional palpation is subjective, experience-based, and thus may be unreliable; for example, for pain location assessment in patients with low back pain, the palpation reliability varies greatly in different tissues: the Kappa values (an indicator of reliability)[34] varies from 0.34 to 0.80 for soft tissues and 0.14 to 0.73 for joint and bony structures.[35] Considering that the identification reliability (Kappa value) of conventional manual palpation on real patients is mostly around 0.4,[35, 36] the Kappa values of our single FSS and tactile glove on identifying the real body features and the simulator were calculated and the tactile glove achieved reliability of 0.98 (Figure 4f and Figure S24), indicating the potential applicability in future healthcare.

3. Conclusions

We presented freestanding and scalable bimodal tactile platforms with FSS arrays, of which the shapes and sizes are customizable according to target subjects, allowing for force and softness sensing in large areas. Relying on this, a thin, conformal, and stretchable tactile glove with 112 FSSs was fabricated, enabling spatial tactile information of force and softness to be digitalized while allowing hand skills to be freely performed. Based on machine learning analysis, the tactile glove identifies body features in a real person and healthy/pathological organ models inside a medical abdominal simulator with high accuracy (98%), indicating the potential value for realizing data-based objective palpation, which would promote the revolution of conventional experience-based and subjective palpation. Due to the freestanding and customizable, our tactile platform is adaptable to various medical devices for digitalized healthy monitoring and haptic interfaces for advanced humanoid robots.

4. Experimental Section/Methods

Performance characterization of tactile sensors and sample fabrication

The resistance of pressure sensors is measured by a 2450 Source Meter (Keithley), and the pressing forces between samples and pressure sensors are controlled by an electromechanical test system (Criterion 42, MTS). The thermal property of the piezoresistive film was measured by a differential scanning calorimeter (Q10, TA Instruments). The profile of the hot-pressed piezoresistive film and the coaxial circular electrodes were measured by a surface profiler (Alpha-Step D-500 Stylus Profiler, KLA). The surface of the copper electrode is characterized by a 3D surface metrology microscope (DCM8, Leica).

PDMS samples for softness identification experiments were fabricated with the different base-to-curing agent ratios, followed by curing in an oven (Binder) at 60 °C for 5 h. Ecoflex 00-10, 00-30, and 00-50 (Smooth-On) samples were fabricated by mixing equal volumes of Part A and Part B, followed by curing at room temperature. The fabrication yields standard samples with a series of Young's modulus (37 kPa, 60 kPa, 89 kPa, 189 kPa, 326 kPa, 1046 kPa), which is measured under standard tensile tests by the MTS.

The fabrication of the FSS on PET substrate began with adhering the PET substrate to a transparent poly(methyl methacrylate) (PMMA) board, followed by covering a piece of black commercial piezoresistive films (Velostat, 3M) on the circular interdigital Cr/Au electrodes. This hinders the observation of the interdigital electrode beneath the piezoresistive film from the front view. To ensure the exact location of a pair of electrodes, a pair of perpendicular lines were drawn from the back of the PMMA board, and the intersection point marks the location. Then another pair of perpendicular lines were drawn from the front view of the PMMA board by following the lines of the backside. Thus the intersection point locates the center of the interdigital electrodes beneath the piezoresistive film. A protrusion made of elastic silicone glue (Sil-Poxy, Smooth-On) was fabricated from a 3D-printed mold (Veroblue, Stratasys) using a commercial 3D printer (Eden260V, Stratasys) (Figure S13c) and adhered to the piezoresistive film above the intersection point.

All protrusions with different softness and different morphologies were fabricated using corresponding materials (PDMS, Ecoflex, and Sil-Poxy) and cured in the corresponding 3D-printed molds. The 3D-printed molds were sprayed with a release agent before the uncured materials filled the molds.

The fabrication of PDMS pyramid pressure sensors began with pouring uncured PDMS (10:1) on a reversed pyramid microstructured silicon mold, followed by peeling off after curing (60 °C for 12 h). The PDMS micro-structured film was treated with oxygen plasmon (350 W, 2 min) and followed by placing it on a hot plate of 120°. The CNT water solution (P3-SWNT,

Carbon Solution) of 0.1 mg/mL was then spray-coated on the PDMS film. The CNT/PDMS film was then placed on a PET film with a pair of interdigital electrodes (Cr (3 nm)/Au (100 nm)), forming the pressure sensor.

The fabrication process of the tactile glove

Fabrication of the hand-shaped FPC. Fabrication of the stretchable circuit begins with patterning a thin and flexible film (Hubei Heng Chi Electronic Technology Co., Ltd) of copper/PI/copper (18 μm/13 μm/18 μm) into hand-shaped FPC with 113 buried electrodes (1 common electrode and 112 counter electrodes) and 112 pairs of exposed coaxial circular electrodes according to standard industrial process.

Adhering pressure sensors on the hand-shaped FPC. The hand-shaped FPC was first cleaned by ultrasonic in DI water, ethanol, acetone, and oxygen plasma treatment in sequence, followed by immersing in 2-mercaptoethanol (Sigma-Aldrich)/ethanol solution (20 μL/1 L) for 12 h to decorate the gold surface. The piezoresistive film (Velostat, 3M) was punctured into disc-shaped (2 mm in diameter) before being treated with oxygen plasma. The disc-shaped piezoresistive films were then adhered to the exposed coaxial circular gold electrodes by hot-press (1 MPa, 90 ℃, 10 s). The pressure sensors were further sealed on the hand-shaped FPC by the elastic silicone glue (Sil-Poxy, Smooth-On), as shown in Figure S13a.

Fabrication of tactile gloves. A highly stretchable commercial textile glove that is fabricated with polyamide and polyurethane fibers is worn on a hand model (PMMA) cut by a laser machine (VLS360DT, Universal), and then sealed by a layer of Ecoflex 00-10 (Smooth-On) on the front side. The hand-shaped FPC is then adhered to the textile glove using the Sil-Poxy, followed by adhering hemispherical protrusions on the pressure sensors. All protrusions were made of Sil-Poxy using a 3D-printed mold, which was printed by Eden260V (Stratasys) using commercial UV-curable materials (VeroBlue, Stratasys).

Data collection and tactile imaging.

Design of the massive analog signal channels-based flexible printed circuit board (MASC-FPCB). The MASC-FPCB is designed as a flexible wearable board. The circuit includes a power management module for generating a stable reference voltage V_{ref} and supplying power to the microprocessor unit (MCU) and its auxiliary universal asynchronous receiver transmitter (UART) to the universal serial bus (USB) module (Figure S25a).

To avoid crosstalk and proximity effects, a corresponding sampling circuit is designed for each sensor. The passive matrix and coaxial circular electrodes design of the sensor array makes the fabrication simple, and the design is adaptable to multiple platforms. Any damage to a single sensor does not influence other sensors, eliminating possible parasitic effects.

Moreover, each sampling circuit channel can be optimized individually, and no amplifier components are needed.

The charging resistor arrays R_{c1} to R_{cn} are required, and the corresponding R_c is designed according to the resistance range of the corresponding sensor, which ensures the optimal working status of the sampling circuit in each channel and reduces noise. The MASC-FPCB is shown in Figure S25b, with two 60-pin FPC connectors connecting with the sensor array of the tactile glove via the hand-shaped FPC.

Data readout and imaging. All sensors are divided into 16 different groups, and each group is connected with a 7-channel sampling circuit (Figure S25a). Each channel can be selected by controlling the analog switch via the MCU. One channel of each group is selected at a time to collect sensor values. The single-chip MCU controls 16 analog switches at the same time. In this way, the resistance of 16 sensors can be collected at the same time as sampling, and 112 sensors can be collected under 7 cycles of scanning. Thus, the scan period for the sensor array can be greatly reduced. The 16 sensor measurements at the output of the 16 analog switches are converted to a digital signal (10-bit resolution; 0–1,023 corresponding to 0–5 V). The collected data are then transmitted to the host computer through the serial communication protocol for further processing and imaging (Figure S25c).

On-body tests

The tests on the human body done at Nanyang Technological University were approved by the Institute of Review Board, Nanyang Technological University, and following informed written consent (approval number: IRB-2017-08-035).

Tests with the abdominal simulator

A commercial abdominal simulator for examination in medical education (AbdoAbby, Kyoto Kagaku) is used for the validation of intelligent palpation. Figure S26 shows the abdominal simulator and corresponding organ models for testing. Pathological liver (pre-cirrhosis) and spleen models are slightly larger than healthy models, leading to harder feeling compared with healthy organ models when pressing on the corresponding locations of the simulator.

Machine learning

A support vector machine is adopted to learn the classifier to predict the class labels based on the measured data. The dataset includes 8 types with a total of 1800 samples, which was split into train set (1440 samples) and test set (360 samples) for learning the model parameters and evaluating the prediction accuracy, separately. Classification accuracy was used as the metric to evaluate the model performance during training and prediction. For each

training/prediction process, each input sample has 224 features, which include intensity and time signals extracted from the measured data of 112 sensors of the tactile glove system. The intensity feature is the maximum change of the measured resistance during a pressing process, while the time feature is the duration of the intensity signal that is above 85% of the intensity feature (Figure S23).

Supporting Information

Supporting Information is available from the Wiley Online Library or from the author.

Acknowledgements

Z.C., W.W., H.X. contributed equally to this work. The project was supported by Singapore Ministry of Education (MOE2019-T2-2-022) and the National Research Foundation, Singapore (NRF) under NRF's Medium Sized Centre: Singapore Hybrid-Integrated Next-Generation μ-Electronics (SHINE) Centre funding programme. Any opinions, findings and conclusions or recommendations expressed in this material are those of the author(s) and do not reflect the views of National Research Foundation, Singapore (NRF).

Received: ((will be filled in by the editorial staff))
Revised: ((will be filled in by the editorial staff))
Published online: ((will be filled in by the editorial staff))

References

[1] J. C. Yang, J. Mun, S. Y. Kwon, S. Park, Z. Bao, S. Park, *Adv. Mater.* **2019**, *31*, 1904765.

[2] C. Dagdeviren, Y. Shi, P. Joe, R. Ghaffari, G. Balooch, K. Usgaonkar, O. Gur, P. L. Tran, J. R. Crosby, M. Meyer, Y. Su, R. C. Webb, A. S. Tedesco, M. J. Slepian, Y. Huang, J. A. Rogers, *Nat. Mater.* **2015**, *14*, 728.

[3] E. Song, Z. Xie, W. Bai, H. Luan, B. Ji, X. Ning, Y. Xia, J. M. Baek, Y. Lee, R. Avila, H.-Y. Chen, J.-H. Kim, S. Madhvapathy, K. Yao, D. Li, J. Zhou, M. Han, S. M. Won, X. Zhang, D. J. Myers, Y. Mei, X. Guo, S. Xu, J.-K. Chang, X. Yu, Y. Huang, J. A. Rogers, *Nat. Biomed. Eng.* **2021**, *5*, 759.

[4] M. Wang, Z. Yan, T. Wang, P. Cai, S. Gao, Y. Zeng, C. Wan, H. Wang, L. Pan, J. Yu, S. Pan, K. He, J. Lu, X. Chen, *Nat. Electron.* **2020**, *3*, 563.

[5] X. Yu, H. Wang, X. Ning, R. Sun, H. Albadawi, M. Salomao, A. C. Silva, Y. Yu, L. Tian, A. Koh, C. M. Lee, A. Chempakasseril, P. Tian, M. Pharr, J. Yuan, Y. Huang, R. Oklu, J. A. Rogers, *Nat. Biomed. Eng.* **2018**, *2*, 165.

[6] C. Wang, B. Qi, M. Lin, Z. Zhang, M. Makihata, B. Liu, S. Zhou, Y. H. Huang, H. Hu, Y. Gu, Y. Chen, Y. Lei, T. Lee, S. Chien, K. I. Jang, E. B. Kistler, S. Xu, *Nat. Biomed. Eng.* **2021**, *5*, 749.

[7] Z. Cui, W. Wang, L. Guo, Z. Liu, P. Cai, Y. Cui, T. Wang, C. Wang, M. Zhu, Y. Zhou, W. Liu, Y. Zheng, G. Deng, C. Xu, X. Chen, *Adv. Mater.* **2022**, *34*, 2104078.

[8] S. Chun, J.-S. Kim, Y. Yoo, Y. Choi, S. J. Jung, D. Jang, G. Lee, K.-I. Song, K. S. Nam, I. Youn, D. Son, C. Pang, Y. Jeong, H. Jung, Y.-J. Kim, B.-D. Choi, J. Kim, S.-P. Kim, W. Park, S. Park, *Nat. Electron.* **2021**, *4*, 429.

[9] Z. Lv, C. Wang, C. Wan, R. Wang, X. Dai, J. Wei, H. Xia, W. Li, W. Zhang, S. Cao, F. Zhang, H. Yang, X. Loh, X. Chen, *Adv. Mater.* **2022**, *34*, 2202877.

[10] W. W. Lee, Y. J. Tan, H. Yao, S. Li, H. H. See, M. Hon, K. A. Ng, B. Xiong, J. S. Ho, B. C. Tee, *Sci. Robot.* **2019**, *4*, eaax2198.

[11] W. Li, N. Matsuhisa, Z. Liu, M. Wang, Y. Luo, P. Cai, G. Chen, F. Zhang, C. Li, Z. Liu, Z. Lv, W. Zhang, X. Chen, *Nat. Electron.* **2021**, *4*, 134.

[12] Y. Zhai, Z. Wang, K. S. Kwon, S. Cai, D. J. Lipomi, T. N. Ng, *Adv. Mater.* **2020**, *33*, 2002541.

[13] X. Yu, Z. Xie, Y. Yu, J. Lee, A. Vazquez-Guardado, H. Luan, J. Ruban, X. Ning, A. Akhtar, D. Li, B. Ji, Y. Liu, R. Sun, J. Cao, Q. Huo, Y. Zhong, C. Lee, S. Kim, P. Gutruf, C. Zhang, Y. Xue, Q. Guo, A. Chempakasseril, P. Tian, W. Lu, J. Jeong, Y. Yu, J. Cornman, C. Tan, B. Kim, K. Lee, X. Feng, Y. Huang, J. A. Rogers, *Nature* **2019**, *575*, 473.

[14] I. You, D. G. Mackanic, N. Matsuhisa, J. Kang, J. Kwon, L. Beker, J. Mun, W. Suh, T. Y. Kim, J. B.-H. Tok, Z. Bao, U. Jeong, *Science* **2020**, *370*, 961.

[15] S. Lee, S. Franklin, F. A. Hassani, T. Yokota, M. O. G. Nayeem, Y. Wang, R. Leib, G. Cheng, D. W. Franklin, T. Someya, *Science* **2020**, *370*, 966.

[16] W. Yuan, M. A. Srinivasan, E. H. Adelson, presented at *IEEE Int. Conf. Intell. Robots Syst.*, Daejeon, (10, **2016**).

[17] C. Dhong, R. Miller, N. B. Root, S. Gupta, L. V. Kayser, C. W. Carpenter, K. J. Loh, V. S. Ramachandran, D. J. Lipomi, *Sci. Adv.* **2019**, *5*, eaaw8845.

[18] Y. Wu, Y. Liu, Y. Zhou, Q. Man, C. Hu, W. Asghar, F. Li, Z. Yu, J. Shang, G. Liu, *Sci. Robot.* **2018**, *3*, eaat0429.

[19] W. Heng, S. Solomon, W. Gao, *Adv. Mater.* **2022**, *34*, 2107902.

[20] J. Wang, C. Wang, P. Cai, Y. Luo, Z. Cui, X. J. Loh, X. Chen, *ACS Nano* **2021**, *15*, 18671.

[21] A. S. Naidu, M. D. Naish, R. V. Patel, *IEEE Robot. Autom. Mag.* **2017**, *24*, 54.

[22] T. Belpaeme, J. Kennedy, A. Ramachandran, B. Scassellati, F. Tanaka, *Sci. Robot.* **2018**, *3*, eaat5954.

[23] C. Breazeal, presented at *Annu. Int. Conf. IEEE Eng. Med. Biol.* Boston, (8, **2011**).

[24] R. Kirby, J. Forlizzi, R. Simmons, *Rob. Auton. Syst.* **2010**, *58*, 322.

[25] E. Nagy, T. Farkas, F. Guy, A. Stafylarakis, *Percept. Mot. Skills* **2020**, *127*, 52.

[26] P.-H. Orefice, M. Ammi, M. Hafez, A. Tapus, presented at *IEEE-RAS Int. Conf. Humanoid Robots*, Cancun, (11, **2016**).

[27] S. Sundaram, P. Kellnhofer, Y. Li, J.-Y. Zhu, A. Torralba, W. Matusik, *Nature* **2019**, *569*, 698.

[28] Y. Luo, Y. Li, P. Sharma, W. Shou, K. Wu, M. Foshey, B. Li, T. Palacios, A. Torralba, W. Matusik, *Nat. Electron.* **2021**, *4*, 193.

[29] G. Li, S. Liu, L. Wang, R. Zhu, *Sci. Robot.* **2020**, *5*, eabc8134.

[30] S. McKinley, A. Garg, S. Sen, R. Kapadia, A. Murali, K. Nichols, S. Lim, S. Patil, P. Abbeel, A. M. Okamura, K. Goldberg, presented at *IEEE Int. Conf. Autom. Sci. Eng.*, Gothenburg, (8, **2015**).

[31] H. Zhao, K. O'Brien, S. Li, R. F. Shepherd, *Sci. Robot.* **2016**, *1*, eaai7529.

[32] L. Beker, N. Matsuhisa, I. You, S. R. A. Ruth, S. Niu, A. Foudeh, J. B.-H. Tok, X. Chen, Z. Bao, *Proc. Natl. Acad. Sci.* **2020**, *117*, 11314.

[33] B. C. K. Tee, A. Chortos, R. R. Dunn, G. Schwartz, E. Eason, Z. Bao, *Adv. Funct. Mater.* **2014**, *24*, 5427.

[34] M. Haas, *J. Manip. Physiol. Ther.* **1991**, *14*, 119.

[35] P. S. Nolet, H. Yu, P. Cote, A. L. Meyer, V. L. Kristman, D. Sutton, K. Murnaghan, N. Lemeunier, *Chiropr. Man. Ther.* **2021**, *29*, 33.

[36] A. Jonsson, E. Rasmussen-Barr, *Physiother. Theory Pract.* **2018**, *34*, 165.

Freestanding and scalable tactile platforms with force-softness bimodal sensor arrays are developed, enabling a tactile glove to digitalize pressing force and softness in large areas of the human body. Combining with machine learning methods, the tactile glove identifies body features in a real person and a medical abdominal simulator with high accuracy (98%).

Zequn Cui, Wensong Wang, Huarong Xia, Changxian Wang, Jiaqi Tu, Shaobo Ji, Joel Ming Rui Tan, Zhihua Liu, Feilong Zhang, Wenlong Li, Zhisheng Lv, Zheng Li, Wei Guo, Nien Yue Koh, Kian Bee Ng, Yuanjin Zheng*, Xiaodong Chen*

Freestanding and scalable force-softness bimodal sensor arrays for haptically body feature identification